半導体スピン注入を用いた核スピンのコヒーレント制御

秋保貴史，蝦名優也，山本眞史，植村哲也
（北海道大学）

Coherent control of nuclear spins using spin injection into semiconductor

T. Akiho, Y. Ebina, M. Yamamoto and T. Uemura,
(Hokkaido University)

はじめに

近年，強磁性体電極から半導体に注入された電子スピンにより核スピンを効率的に偏極する動的核スピン偏極(DNP)，及び，核磁気共鳴(NMR)による核スピン制御が量子情報デバイスへの応用の観点から注目されている．最近，我々は，ホイスラー合金 Co_2MnSi (CMS)から GaAs への高効率なスピン注入と，注入された電子スピンを用いた高効率な DNP を実証した[1,2]．本研究の目的は，半導体スピン注入技術を利用し，NMR による核スピンのコヒーレント制御を実証することである．

実験方法

CMS 電極をスピン源，n 型 GaAs をチャネルとするスピン注入素子に対し，4 端子非局所配置にて，大きさ 114 mT の静磁場($\mathbf{B_0}$)を Fig. 1 に示すように z 軸から約 5 度傾けた方向に印加し，460 秒間待機した．注入電流(I)は 90 μA であり，このとき，DNP により生成される核磁場と外部磁場が打ち消しあい，電子スピンに作用する有効磁場はほぼゼロとなる．この状態を初期状態として，周波数 f = 1150 kHz の正弦波高周波磁場($\mathbf{B_{ac}}$)を時間 τ_p の間印加したときの非局所電圧(V_{NL})変化を計測した．$\mathbf{B_{ac}}$ の周波数は ^{69}Ga に対する NMR の共鳴周波数に相当する．なお，測定はすべて 4.2 K で行った．

結果および考察

Fig. 2 に τ_p = 56, 112 μsec の $\mathbf{B_{ac}}$ パルス照射後の V_{NL} の時間変化を示す．V_{NL} は RF パルス照射により ΔV_{NL} だけ変化し，その後，数百秒の時間スケールで初期状態まで回復した．V_{NL} の急峻な変化は，^{69}Ga の核磁場が NMR により変化することで，電子スピンに作用する有効磁場が増大し，その結果，電子スピンの歳差運動が誘起されたために生じたものと考えられる．さらに，Fig. 3 に示すように，ΔV_{NL} は τ_p に対し明瞭に振動し，このことは，核スピンの $\mathbf{B_0}$ 方向の成分が高周波磁場印加によりコヒーレントに振動すること，すなわち，核スピン系に形成された量子準位間の Rabi 振動を意味する[3]．半導体スピン注入を用いた Rabi 振動の実証は本研究が初めてであり，量子 Hall 素子を用いた従来研究[4]に比べ，低磁場，かつ，高温での実証は，デバイス応用上，有用と考えられる．

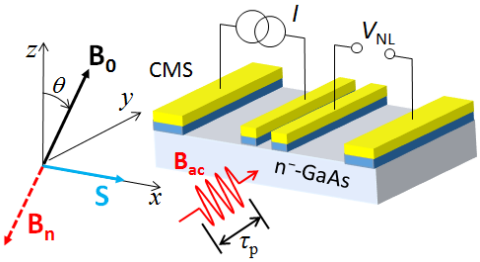

Fig. 1. Schematic diagram of device structure and circuit configuration.

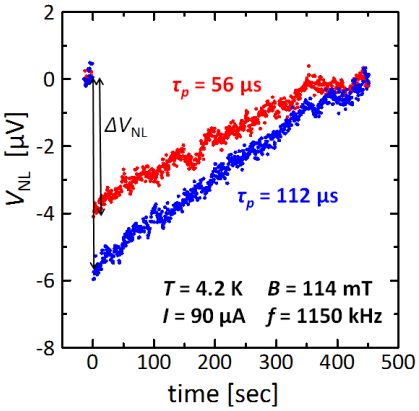

Fig. 2. Time evolution of V_{NL}. Pulsed rf-magnetic field with duration of 56 μs (blue curve) and 112 μs (red curve) was applied at t = 0.

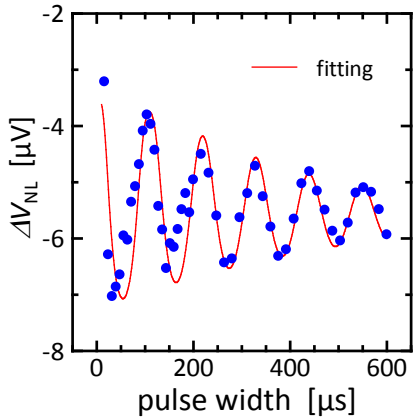

Fig. 3. ΔV_{NL} vs. τ_p (Rabi oscillation).

参考文献

[1] Y. Ebina et al., APL **104**, 172405 (2014).　[2] T. Akiho et al., PRB **87**, 235205 (2013).　[3] T. Uemura et al., PRB **91**, 140410(R) (2015).　[4] T. Machida et al., APL **82**, 409 (2003).

Sb δ-doping of non-degenerate Ge(001) for a spin-FET with a high-mobility channel

T. Takada[1,2], H. Saito[1], A. Spiesser[1], R. Jansen[1], S. Yuasa[1], and N. Miura[2]
([1]AIST, Spintronics Research Center, [2]Meiji Univ.)

Introduction

Spin-dependent transport in a lateral semiconductor (SC) channel with two ferromagnetic (FM) contacts is the fundamental operation principle of the spin field-effect-transistor (spin-FET). For an effective transport of the spin-polarized carriers, the use of a non-degenerate SC is desirable because longer spin lifetimes are expected. The major requirement to employ a non-degenerate SC channel is to suppress the thermionic emission current and enhance the tunneling transport across the FM/SC contact by reducing the depletion region width in the SC region [1]. Recently, Hamaya and his co-workers have developed low-resistance FM tunnel contacts on *n*-type non-degenerate Ge(111) using the Sb δ-doping and low-temperature Ge homoepitaxy [2, 3]. On the other hand, Ge(001) is also a promising candidate as a channel of the spin-FET since epitaxial FM/MgO(001) tunnel barrier can be easily grown, providing a canonical spin injector/detector. Here, we have investigated the effect of the Sb δ-doping on the electrical transport process of Fe/MgO/non-degenerate Ge(001) devices.

Sample preparations

Films were grown by molecular beam epitaxy on *n*-type Ge(001) substrates (a carrier concentration of ~ 5×10^{16} cm^{-3}). Sb was evaporated at room temperature (RT), followed by a 10 nm-thick Ge layer. We prepared several samples with different sheet doping densities of Sb (n_{Sb}) and growth temperature (T_g) of the homoepitaxial Ge layer. Finally, Au(20 nm) / Fe(5 nm) / MgO(1.5 nm) layers were deposited at RT. Reflection high-energy electron diffraction (RHEED) image revealed that the MgO layers have (001)-oriented single-crystalline or textured structure depending on T_g and n_{Sb}.

Results

Figure 1(a) shows the current-voltage (*I*-*V*) characteristics of the devices grown at different T_g with a constant n_{Sb} = 2.0 × 10^{14} cm^{-2}. The devices with T_g = 400 °C and 350 °C reveal a clear rectifying behavior, showing that the thermionic emission is the dominant transport process. With decreasing T_g, the current under reverse bias dramatically increases, and the rectifying behavior finally disappears above T_g = 250 °C. For the devices with T_g = 250 °C and 200 °C, there is no large difference in the resistance-area products (*RA*) as plotted in Fig.1 (b). This indicates that tunneling becomes the major transport process for $T_g \leq 250$ °C.

References

[1] R. Jansen and B. C. Min, Phys. Rev. B **99**, 246604 (2007). [2] K. Sawano *et al.*, Appl. Phys. Lett. **97**, 162108 (2010). [3] K. Kasahara *et al.*, J. Appl. Phys. **111**, 07C503 (2012).

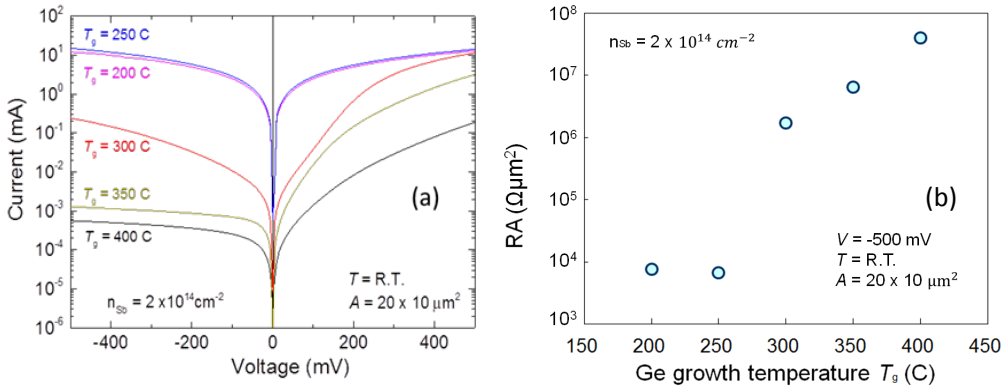

Fig.1 (a) Current-voltage characteristics of Fe/MgO/n-Ge(001) devices and (b) the corresponding *RA* at -500 mV as a function of T_g measured at RT. The sheet Sb doping density n_{Sb} is kept constant with a 2.0 × 10^{14} cm^{-2}.

非弾性散乱トンネルスペクトロスコピーを用いた n-Si/MgO/CoFe 接合中のスピン依存伝導機構の解析

井口智明，石川瑞恵，杉山英行，斉藤好昭
（東芝・研究開発センター）

Spin-dependent transport mechanisms in n-Si/MgO/CoFe junctions investigated by inelastic tunneling electron spectroscopy

T. Inokuchi, M. Ishikawa, H. Sugiyama, Y. Saito
(Corporate R&D Center, Toshiba Corporation)

はじめに

スピン MOSFET に代表される半導体スピントロニクスデバイスでは，強磁性体と半導体の間でのスピン注入/検出効率がデバイスの性能を決めるキーパラメータとなる。理想的な状況においては，半導体/トンネルバリア/強磁性体接合におけるスピン注入/検出効率は強磁性体中の電子のスピン偏極率，トンネルバリアでのスピン選択率およびコンダクタンスマッチング条件によって決まるはずであるが，現実の系ではそれらのパラメータから予測される値とは異なったスピン注入/検出効率が観測される場合があり（特に 3 端子 Hanle 信号），その要因として接合中の欠陥準位などに起因した 2 ステップトンネリングやトンネル確率の磁場依存性等の影響が指摘されている。今回はそれらの要因がスピン依存伝導に与えている影響を解明し，スピン注入/検出効率を高めるための手がかりを得ることを目的として研究を行った。

実験方法

本研究では n-Si 基板/MgO (2.2 nm)/CoFe/Ru からなる接合に対して，直流 Hanle 効果測定を行い，その後同試料に対して非弾性散乱トンネルスペクトロスコピーを行った。非弾性散乱トンネルスペクトロスコピーを行う際には，接合に対して直流バイアス電圧と交流電圧を印加して 2 階微分コンダクタンスを測定し，その 2 階微分コンダクタンスの直流バイアス電圧依存性と，その磁場依存性を測定している。

実験結果

図 1 に直流 Hanle 効果測定の結果を示す。本試料においては主に低バイアス領域で半値幅の大きい，すなわち，電子のスピン寿命が短いことを意味する Hanle 信号と，高バイアス領域で半値幅の小さい，すなわち，電子のスピン寿命が長いことを意味する Hanle 信号の 2 種類の成分が観測される。つまり，本研究で用いた接合ではスピン寿命の異なる伝導機構が存在していると解釈することができる。次に，本接合の 2 階微分コンダクタンスの直流バイアス電圧および磁場依存性を測定した結果を図 2 に示す。2 階微分コンダクタンスは直流 Hanle 効果と同様にローレンツ型の磁場依存性を示し，その半値幅は直流 Hanle 効果測定で観測された半値幅の広い成分のものとほぼ一致する。これらの結果は，半値幅の広い Hanle 信号は接合中の欠陥準位によって非弾性散乱される伝導パスにおいて観測されていることを示唆している。本発表ではこれらの結果について述べると共に，これらの知見からスピン注入/検出効率を高めるための道筋について考察した結果を述べる。なお，本研究の一部は科学研究費補助金（基盤研究 (A) 25246020）の支援を受けて行ったものである。

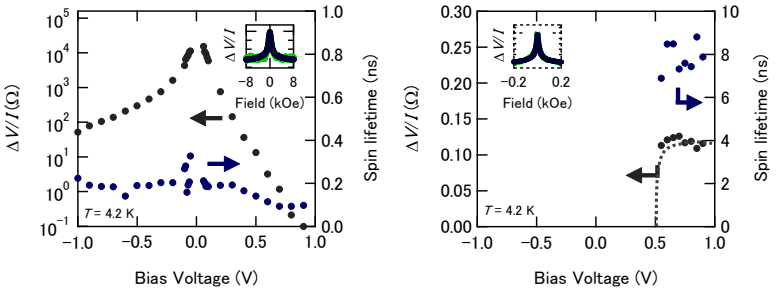

図 1. 直流 Hanle 信号の直流バイアス電圧依存性

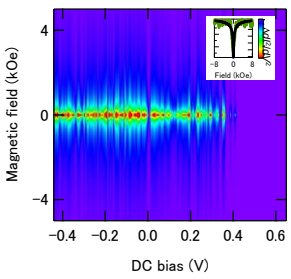

図 2. 2 階微分コンダクタンスの直流バイアス電圧および外部磁場依存性

参考文献

1) R. Jansen *et al.*, Phys. Rev. B **85**, 134420 (2012). 2) Y. Song *et al.*, Phys. Rev. Lett. **113**, 047205 (2014).
3) T. Inokuchi *et al.*, Appl. Phys. Lett. 105, 232401 (2014).

$Co_2FeSi_{0.5}Al_{0.5}/n^+$-Ge ショットキートンネル接合を用いた *n*-Ge 中の室温スピン伝導検出

藤田裕一[1]，岡孝保[1]，山田晋也[1]，山田道洋[2]，澤野憲太郎[3]，金島岳[1]，浜屋宏平[1]
([1]阪大基礎工，[2]慶應理工，[3]東京都市大工)

Spin transport in *n*-Ge at room temperature by using $Co_2FeSi_{0.5}Al_{0.5}/n^+$-Ge Schottky-tunnel contacts

Y. Fujita[1], T. Oka[1], S. Yamada[1], M. Yamada[2], K. Sawano[3], T. Kanashima[1], K. Hamaya[1]
([1]Graduate School of Engineering Science, Osaka Univ., [2]School of Fundamental Science and Technology, Keio Univ., [3]Advanced Research Laboratories, Tokyo City Univ.)

【はじめに】

Ge チャネルスピントランジスタの実現のためには，Ge への電気的スピン注入・検出が必要不可欠である．これまで我々は，低温分子線エピタキシー(MBE)法を用いて *n*-Ge 上にホイスラー合金 Co_2FeSi(CFS)を高品質に形成し，それを用いて Ge 中のスピン伝導の電気的検出に成功してきた[1]．しかし，それは 200 K 程度の低温に留まっており，未だ室温での観測には至っていない．今回，室温での高いスピン機能が実証されているホイスラー合金 $Co_2FeSi_{0.5}Al_{0.5}$(CFSA)[2]を Ge 上に高品質に形成することに成功し，それを利用した室温スピン伝導の電気的検出を報告する．

【実験方法】

Ge(111) 基板上に，*n*-Ge チャネル層(~50 nm)と n^+-Ge 層 (~5 nm、~10^{19} cm^{-3})をそれぞれ形成後，MBE 法による Co，Fe，Si，および Al の非化学量論組成比での同時蒸着[3]により，CFSA 薄膜(10 nm)を室温形成した．その上に電子線蒸着法により Co 層(20 nm)を形成し，Co/CFSA/n^+-Ge/*n*-Ge 構造とした．電子線リソグラフィおよび Ar^+ミリングを用いて，この試料を横型素子構造へと加工した．

【実験結果】

Fig. 1 の断面 TEM 像から急峻な CFSA/Ge ヘテロ接合の実現が確認され，CFSA 膜中の電子線回折パターンからは，$L2_1$ 構造の形成が示唆された．つまり，室温での高いスピン機能が期待できる，高品質な CFSA を Ge 上に形成することに成功したと言える．

Fig. 2 に，T = 300 K，電流値 I = +2.5 mA における四端子非局所磁気抵抗の面内磁場依存性を示す．Co/CFSA 電極の磁化配置が平行(↑↑)・反平行(↑↓)状態において，約 36 mΩ の非局所磁気抵抗の変化(非局所スピン信号)を観測することに成功した．

本研究の一部は、革新的研究開発推進プログラム(ImPACT)及び科研費基盤研究(A)(No. 25246020) からの支援を受けて行われた．

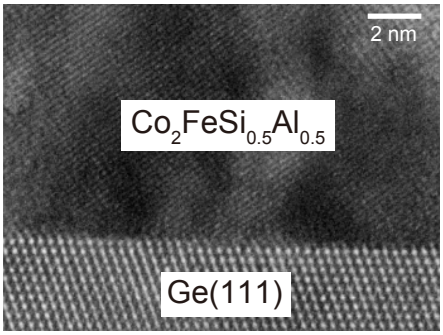

Fig. 1 Cross sectional TEM image of a CFSA/Ge(111) heterojunction.

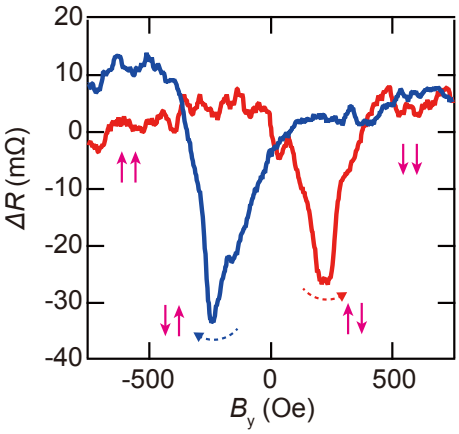

Fig. 2 Nonlocal magnetoresistance curve at 300 K.

参考文献

[1] K. Kasahara *et al.*, Appl. Phys. Express **7,** 033002 (2014).
[2] N. Tezuka *et al.*, Appl. Phys. Lett. **94**, 162504 (2009).
[3] K. Tanikawa *et al.*, Thin Solid Films **557**, 390-393 (2014).

CoFe/TiO_2/Si トンネルコンタクト型スピン注入源における ラジカル酸素アニールの効果

生瀬裕之[1], 悪七泰樹[1], 周藤悠介[1], 高村陽太[2], 菅原聡[1]
([1]東工大像情報, [2]東工大電子物理)

The effect of radical oxygen annealing on CoFe/TiO_2/Si tunnel-contact-type spin injector

Y. Ikuse[1], T. Akushichi[1], Y. Shuto[1], Y. Takamura[2], and S. Sugahara[1]
([1]Imaging Sci. and Eng. Lab., Tokyo Inst. of Tech., [2]Dept. of Physical Electronics, Tokyo Inst. of Tech.)

【はじめに】 電子の持つスピンの自由度を利用してトランジスタの出力特性を制御できるスピン MOSFET[1]などのスピントランジスタが注目されている. スピン MOSFET を実現するためには Si チャネルへのスピン注入および Si チャネルにおけるスピン伝導の実現が必要である. また, スピン MOSFET の実現が期待されるナノスケールのチャネルでは, チャネルのオン抵抗は非常に低く, これまでに研究が進められている AlO_x や MgO をトンネル障壁としたトンネルコンタクト型のスピン注入源では, トンネル抵抗が高く, 抵抗率不整合の問題やトランジスタ性能の劣化といった問題を生じる. そこで, 我々はナノスケールのチャネルに適合した低抵抗スピン注入源として TiO_2 をトンネル障壁として用いたスピン注入源を提案した[2]. この構造では, TiO_2 は Si との接合において Si の伝導帯側に 0.1eV 程度の極めて低いエネルギー障壁を形成[3]できる. これに低仕事関数のハーフメタル $CoFe_2Si_xAl_{1-x}$(CFSA)を強磁性電極に用いることで, 非常に低いトンネル抵抗を実現し, さらに高いスピン注入効率の期待できるスピン注入源となることが予想される. TiO_2 は低抵抗の MTJ のトンネル障壁として研究・開発されていたこともあり, TMR も観測されている[4]. したがって, CFSA/TiO_2/Si トンネルコンタクトはスピン MOSFET のスピン注入源として有望であると考えられる. 今回, 我々は Ti 薄膜のラジカル酸化によって TiO_2 薄膜を形成し, さらにラジカル酸素アニールによって高品質化した TiO_2 薄膜をトンネル障壁とし, CoFe を強磁性電極に用いた CoFe/TiO_2/n^+-Si スピン注入源を作製して, スピン注入の評価を行った. 特に, ラジカル酸素アニールの効果について詳細に調べた.

【実験方法】 TiO_2 は, 超高真空中で熱クリーニングにより清浄表面を露出させた n^+-Si 基板上に Ti をスパッタ堆積した後, 室温でラジカル酸化を行うことで形成した. 室温での Ti の堆積はシリサイドの形成を防ぐためである. 次いで, 形成した TiO_2 に 200-500℃の温度でラジカル酸素アニールを施した. さらに, この表面に CoFe を分子線堆積(MBD)法によって堆積した. これの一連の成膜にはマルチチャンバーシステムを用いて, 試料を大気暴露することなく, すべて超高真空下で行った. 次に, CoFe/TiO_2/n^+-Si トンネルコンタクト構造をスピン注入源とした 3 端子スピン蓄積デバイスを作製した(Fig.1).

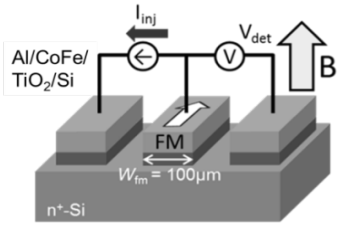

Fig1. Schematic of fabricated 3-terminal spin accumulation device

【実験結果】 はじめに, 室温でラジカル酸化によって形成した TiO_2/Si およびこの構造にラジカル酸素アニール処理を行った試料を XPS によって評価した. Fig. 2(a),(b)に Si2p スペクトルおよび Si サブオキサイドピークの積分値をそれぞれ示す. ラジカル酸化を行うことにより, Si サブオキサイドが形成されるが, これは 100℃でラジカル酸素アニールを行っても変化しなかった(Fig. 2(b)の領域 I). ラジカル酸素アニールを 200℃~400℃で行うと, 領域 I と比較してサブオキサイドのピーク強度が増大するが, この温度範囲内ではピーク強度は一定となり, 界面構造が安定化することが確認された(Fig. 2(b)の領域 II). さらに, アニール温度を増加させると(450℃以上), サブオキサイドピークのピーク強度が増大することが分かった(Fig. 2(b)の領域 III). 次に, この領域 I～III の条件で形成した CoFe/TiO_2/Si トンネルコンタクトをスピン注入源とする 3 端子スピン蓄積デバイスを作製し, スピン注入の評価を行った. 領域 I～III の条件で作製したすべてのデバイスにおいて, スピン注入およびスピン抽出に関する Hanle 効果信号の観測に成功した. 得られた信号はどれも単一の Lorentz 関数ではフィッティングを行うことができず, トラップスピンを表す Lorentz 関数とチャネルスピンを表す関数[5]との重ね合わせによって, 精度よくフィッティングを行うことができた(Fig.3(a)). また, 信号に含まれるトラップスピン成分に対するチャネルスピン成分の割合は, 領域 II の条件で作製したデバイスが最も高くなり(Fig.3(b)), ラジカル酸素アニール温度の最適化によりのスピン注入効率を大幅に改善できることがわかった. 以上の結果から, TiO_2 トンネル障壁は Si チャネルに関するスピン注入源に適用が可能であると考えられる.

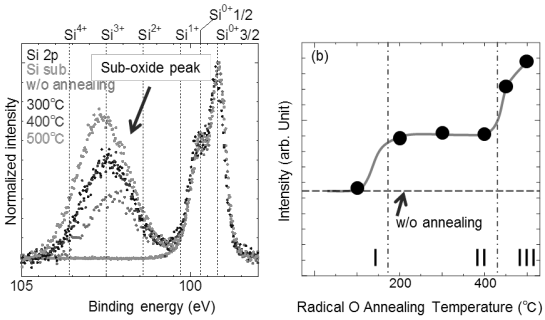

Fig. 2 (a) XPS Si2p spectra of TiO_2/Si samples, in which radical oxygen annealing temperatures are varied. (b) Annealing-temperature dependence of integrated sub-oxide peak intensity of the Si2p spectra.

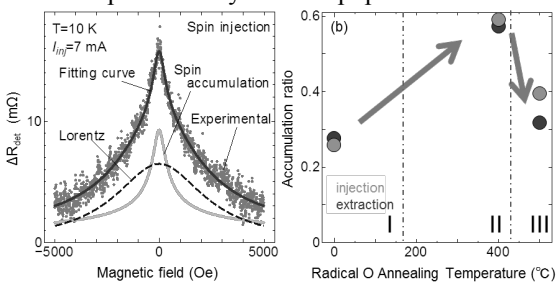

Fig. 3 (a) Hanle-effect signal and its fitting curves for 400 ℃-annealed sample. (b) Intensity ratio for the channel spin component as a function of annealing temperature.

【参考文献】 1). S. Sugahara, IEE Proc. Circuits, Devices & Sys. **152**, 355 (2005). 2). K.Takahashi, *et al*., The 38th Annual conference on MAGNETICS in Japan (2014). 3). J. Robertson, J. Vac. Sci. Technol. B **18**, 1785 (2000). 4). J. Gang. Zhu, and C. Park, Mater. Today, **9**, 36(2006). 5). Y. Takamura, *et al*., J. Appl. Phys. **115**, 17C307 (2014)

純スピン流注入によるホイスラー合金のダンピング変調

沖宗一郎[1]，河野慎[1]，山田晋也[1]，金島岳[1]，能崎幸雄[2,3]，浜屋宏平[1,3]
([1]阪大基礎工，[2]慶大理工，[3]JST-CREST)

Control of the effective damping constant for Heusler alloys by pure spin current

S. Oki[1], M. Kawano[1], S. Yamada[1], T. Kanashima[1], Y. Nozaki[2,3], K. Hamaya[1,3]
([1]Osaka Univ., [2]Keio Univ., [3]JST-CREST)

【はじめに】

近年、マイクロ波アシスト磁化反転の応用として、磁性体への純スピン流注入を利用した実効ダンピング定数の変調が報告されている[1,2]。一方、これまで我々は Si 基板上に作製した $L2_1$-Co_2FeSi(CFS)や $D0_3$-Fe_3Si(FS)を横型スピンバルブ素子へ加工し、高効率に純スピン流を生成・検出する技術を確立してきた[3,4]。本研究では、CFS から高効率に生成された純スピン流を FS へ注入し、FS の実効ダンピング定数を変調する。

【実験手法】

MBE を用いて Si 基板上に作製した膜厚 10nm/15nm の CFS/FS 薄膜を[4]、電子線描画と Ar^+ミリングを用いて CFS/FS および FS 細線に加工し、100nm 膜厚のスピン流伝送路及びコプレーナ線路(CSW)を Cu 蒸着により作製した[2-4](Fig.1)。FMR スペクトルは Fig.1(a)の端子配置でマイクロ波を CSW に加えながら細線長軸方向からθ=10° の方向に外部磁場 H_{ex} を掃引し、整流効果によって細線両端に生じる直流電圧により検出した。純スピン流は Fig.1(b)の端子配置で細線長軸方向に外部磁場 H_{ex} を掃引し、交流電圧を印加してロックインアンプを用いて非局所電圧によって検出した。

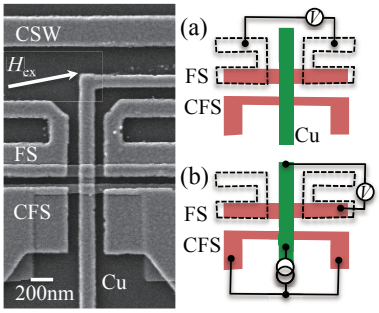

Fig.1 SEM image of the device used and schematic images of the terminal configurations.

【実験結果】

Fig.2 に 15dBm のマイクロ波における FMR スペクトルの周波数依存性を示す。キッテル式による解析から飽和磁化 M_s=871 emu/cm^3 と見積もられ、FMR 検出電極が高品質な FS[5](~858 emu/cm^3)であることが確認された。Fig.3 に CFS を表面とする CFS/FS 電極から FS 電極への純スピン流注入の結果を示す。注入・検出電極の磁化配置に対応した明瞭なヒステリシスを有するΔR_S=2.6 mΩのスピン信号が観測された。さらに直流電流を印加し、純スピン流を注入した状態で FMR スペクトルの測定を行ったところ[1,2]、印加電流に応じて FS の実効ダンピング定数が変化することが確認され、変調効率は Py[2]より大きいことが判明した。講演ではダンピング定数の変調とその効率について、詳細に報告する。

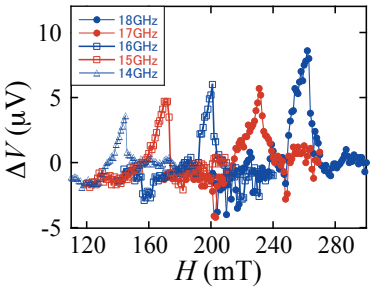

Fig.2 FMR spectra of FS for various frequencies.

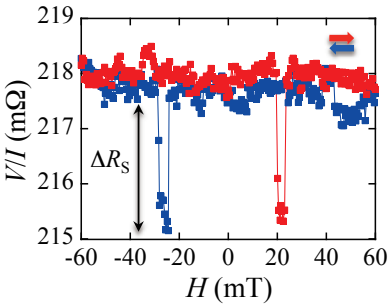

Fig.3 Nonlocal resistance at RT.

本研究の一部は JST CREST、科研費基盤 A(No.25246020)、新学術領域研究ナノスピン変換科学(No.26103003)の支援を受けた。沖および河野は日本学術振興会の支援を受けた。

参考文献

[1] L. Xue *et al.*, Phys. Rev Lett. **108**, 147201 (2012).
[2] Y. Nozaki *et al.*, Appl. Phys. Exp. **8**, 043001 (2015).
[3] K. Hamaya *et al.*, Phys. Rev. B **85**, 100104(R) (2012).
[4] S. Oki *et al.*, Appl. Phys. Lett. **103**, 212402 (2013).
[5] K. Hamaya *et al.*, Phys. Rev. B **83**, 144911 (2011).

Effect of off-stoichiometry on half-metallicity of quaternary Heusler alloy $Co_2(Mn,Fe)Si$ investigated through saturation magnetization and tunneling magnetoresistance

Kidist Moges,[1] Yusuke Honda,[1] Hong-xi Liu,[1] Bing Hu,[1] Tetsuya Uemura,[1] Yoshio Miura,[2] Masafumi Shirai,[3] and Masafumi Yamamoto[1]
[1]Hokkaido University, [2]Kyoto Institute of Technology, [3]Tohoku University

We have recently investigated the effect of off-stoichiometry on the tunneling magnetoresistance (TMR) of the quaternary Heusler alloy $Co_2(Mn,Fe)Si$ (CMFS)-based magnetic tunnel junctions (MTJs) and showed that the (Mn+Fe)-rich composition is critical to suppressing harmful $Co_{Mn/Fe}$ antisites and obtaining half-metallicity [1]. Furthermore, we demonstrated giant TMR ratios of 2610% at 4.2 K and 429% at 290 K for MTJs having Mn-rich, lightly Fe-doped CMFS electrodes [1]. The purpose of the present study was to clarify the origin of the giant TMR ratio of MTJs with Mn-rich, lightly Fe-doped CMFS electrodes. To do this, we experimentally investigated the film composition dependence of the saturation magnetization per formula unit, μ_s, of CMFS films with various compositions of α' and β' in $Co_2(Mn_{\alpha'}Fe_{\beta'})Si_{0.84}$.

Figure 1 shows the film composition dependence of the experimental μ_s of $Co_2(Mn_{\alpha'}Fe_{\beta'})Si_{0.84}$ and $Co_2Mn_{1.40}Si_{0.84}$ films along with the half-metallic Slater-Pauling values (Z_t−24) and the theoretical total spin magnetic moment/f.u., m_{spin}, calculated using the antisite-based site-specific formula unit (SSFU) composition model [1,2]. Although the experimental μ_s was lower than both Z_t−24 and theoretical m_{spin} for Mn-rich $Co_2Mn_{1.40}Si_{0.84}$, its value for $Co_2Mn_{1.24}Fe_{0.16}Si_{0.84}$ in which a small amount of Mn was replaced by Fe for $Co_2Mn_{1.40}Si_{0.84}$ got almost close to the half-metallic Z_t−24. Figure 2 shows how the TMR ratio at 4.2 K of MTJs with Mn-rich, lightly Fe-doped $Co_2Mn_{\alpha'}Fe_{0.16}Si_{0.84}$ electrodes depends on α' ranging from $\alpha' = 1.14$ ($\delta = \alpha' + \beta' = 1.30$) to $\alpha' = 1.24$ ($\delta = 1.40$) along with the dependence of the TMR ratio for CMS MTJs with $Co_2Mn_\alpha Si_{0.84}$ electrodes on the Mn composition α ranging from $\alpha = 0.73$ to 1.40. The drop in the TMR of the CMS MTJ with Mn-rich α =1.40 and the contrasted further increase in the TMR of CMFS MTJs with increasing δ from $\alpha = 1.30$ to 1.40 with a small amount of β' of 0.16 was consistent with the dependence of μ_s shown in Fig. 1. The theoretical m_{spin} values well explained the experimental μ_s values except Mn-rich $Co_2Mn_{1.40}Si_{0.84}$ ($\alpha = 1.40$ CMS). This discrepancy can be attributed to the assumed nominal half-metallic SSFU composition for Mn-rich $\alpha = 1.40$ CMS. Thus, the origin of the giant TMR for MTJs with Mn-rich, lightly Fe-doped CMFS electrodes was attributed to that (1) the nominal half-metallic SSFU composition was recovered by replacing a small amount of Mn by Fe for $\alpha = 1.40$ CMS and (2) the residual $Co_{Mn/Fe}$ antisites were further reduced by (Mn+Fe)-rich composition.

References

[1]. H.-x. Liu et al., J. Phys. D: Appl. Phys. 48, 164001 (2015). [2]. G.-f. Li, et al., Phys. Rev. B 89, 014428 (2014).

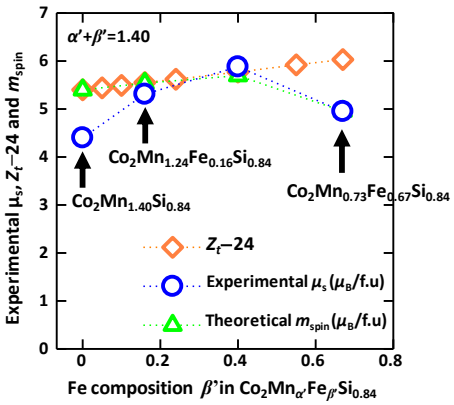

Fig.1. Saturation magnetization per formula unit of $Co_2Mn_{1.40}Si_{0.84}$ and $Co_2Mn_{\alpha'}Fe_{\beta'}Si_{0.84}$ films with $\alpha' + \beta' = 1.40$ in comparison with Slater-Pauling value (Z_t −24) and theoretical m_{spin}.

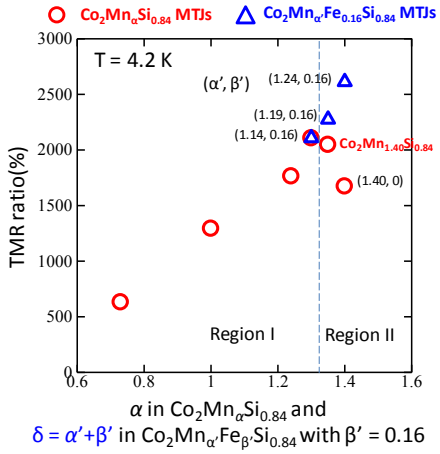

Fig. 2. TMR ratios of CMFS-based MTJs as a function of $\delta = \alpha' + \beta'$ in $Co_2Mn_{\alpha'}Fe_{\beta'}Si_{0.84}$ electrodes and that of identically fabricated CMS-based MTJs as a function of α in $Co_2Mn_\alpha Si_{0.84}$ electrodes.

Characteristic temperature dependence of spin-dependent tunneling conductance of MTJs with highly spin-polarized electrodes

Bing Hu, Kidist Moges, Yusuke Honda, Tetsuya Uemura, and Masafumi Yamamoto
Hokkaido University

Half-metallic ferromagnets are one of the most suitable spin-source materials for spintronic devices because of their complete spin polarization at the Fermi level (E_F). We recently demonstrated that controlling defects through the film composition is critical to retaining the half-metallicity of ternary Heusler alloy Co_2MnSi (CMS) and quaternary alloy $Co_2(Mn,Fe)Si$ (CMFS) [1–3]. As a result, we demonstrated giant TMR ratios for CMS/MgO/CMS magnetic tunnel jucntions (CMS MTJs) and CMFS/MgO/CMFS MTJs (CMFS MTJs) of up to 2610% at 4.2 K and 429% at 290 K [1,3]. The purpose of the present study was to clarify the key mechanisms that determine the temperature (T) dependence of the spin-dependent tunneling conductances G (= I/V) for the parallel (P) and antiparallel (AP), G_P and G_{AP}, in particular, G_P of MTJs with highly spin-polarized electrodes. To do this, we experimentally investigated how the T dependence of G_P and G_{AP} varied with the degree of the half-metallicity of CMS and CMFS electrodes.

The preparation of fully epitaxial CMS MTJs (CMFS MTJs) with various values of α (α' and β') in $Co_2Mn_\alpha Si$ ($Co_2(Mn_{\alpha'}Fe_{\beta'})Si$) electrodes has been described elsewhere [1,3]. The tunneling conductances G_P and G_{AP} were measured by a dc four-probe method at temperatures from 4.2 K to 290 K at a bias voltage of 2 mV.

Figure 1 shows the T dependence of G_P of three kinds of epitaxial MgO-based MTJs: a CMS MTJ and a CMFS MTJ both showing high TMR ratios and an identically prepared $Co_{50}Fe_{50}$ (CoFe)/MgO/CoFe MTJ (CoFe MTJ) showing a relatively low TMR. Contrasting dependences were observed: G_P of the CoFe MTJ increased with increasing T, in particular, for T > 100 K, while G_P of the CMS MTJ and CMFS MTJ decreased with increasing T from T_1 (~25 K) to T_2 (~220 K) and then increased for $T > T_2$. This result suggests the correlation between the T dependence of G_P and the spin polarization at E_F.

The possible origin of the contrasting behaviors of the T dependence of G_P of MTJs featuring a wide range of the TMR ratio at 4.2 K can be explained by the competition between two factors involved in the tunneling mechanisms: One is a spin-flip tunneling process via a thermally excited magnon (Zhang's term) [4], which increases G_P with increasing T, and another is a spin-conserved tunneling process but under the decrease in the tunneling spin polarization, which decreases G_P with increasing T due to a spin-wave excitation (Shang's term) [5]. Note that the contribution to G_P from the Zhang's term decreased with increasing spin polarization. Thus, it is reasonable to ascribe the increase in G_P for MTJs showing lower TMR ratios to the Zhang's term and ascribe the decrease in G_P for a T range from $T_1 < T < T_2$ for MTJs showing higher TMR ratios to the Shang's model because of the relative decrease in the contribution from the Zhang's term. Given these consideration, we fitted the T dependence of G_P of MTJs showing high TMR ratios by taking into account both two factors: Shang's term responsible for the decrease in G_P for $T_1 < T < T_2$ while the Zhang's term responsible for the increase in G_P for $T > T_2$ (Fig. 2). We confirmed that the thus fitted curve well reproduced the $G_P(T)$ for a CMS MTJ showing a giant TMR ratio.

[1] H.-x. Liu et al., Appl. Phys. Lett. **101**, 132418 (2012). [2] G. -f. Li et al., PRB **89**, 014428 (2014). [3] H. -x. Liu et al., J. Phys. D: Appl. Phys. **48**, 164001 (2015). [4] S. Zhang et al., PRL **79**, 19 (1997). [5] C. H. Shang et al., PRB **58**, 2917(R) (1988).

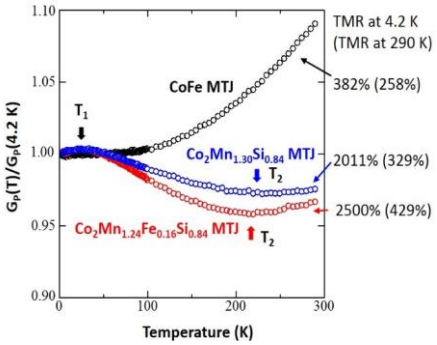

Fig 1. Typical T dependence of the normalized tunneling conductance for P of three kinds of MgO-based MTJs having a wide range of TMR ratio at 4.2 K and 290 K.

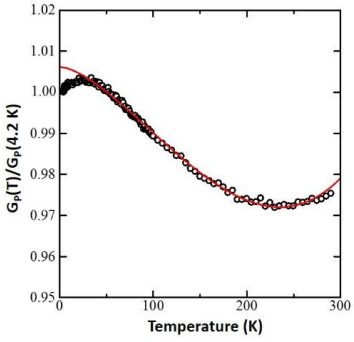

Fig 2. Experimental (open circles) and fitted (line) curve for a $Co_2Mn_{1.30}Si_{0.84}$ MTJ showing giant TMR ratios of 2011% at 4.2 K and 329% at 290 K.

スピンギャップレス半導体のデバイス応用に向けた Mn_2CoAl 薄膜の作製

広瀬慎吾、植田研二、愛知慎也、羽尻哲也、浅野秀文
（名古屋大）

Fabrication of Mn_2CoAl thin films toward device applications for Spin-Gapless-Semiconductors

S. Hirose, K. Ueda, S. Aichi, T. Hajiri, H. Asano+
(Nagoya Univ.)

はじめに

近年注目されているスピンギャップレス半導体(SGS)は片方のスピンを持つ価電子帯と伝導帯がフェルミエネルギー(E_F)の一点で接し、他方スピンを持つバンドは E_F においてバンドギャップとなっているという特殊なバンド構造を有しており高い分極率と高移動度を併せ持つ為、スピントロニクスデバイス材料として非常に有望である。本研究では SGS であると理論予測されている材料のうち、バルクにおいて既に SGS に特有の伝導特性（線形 MR，高移動度 etc.)が観測されている Mn_2CoAl(MCA)に着目し、デバイスに必須となる薄膜化を試みた。

実験方法

MCA 薄膜の作製は格子ミスマッチの小さな MgO (2.7%)及び $MgAl_2O_4$ (1.5%) 基板上にイオンビームアシストスパッタ(IBAS)法 [1]を用いて行った。IBAS 法は製膜中にアシストイオンガンを補助的に用いることで低温での成長が可能となり、界面反応やミキシングを抑えることができる手法である。X 線回折法により結晶構造、試料振動型磁力計(VSM)により磁気特性、四端子法により電気抵抗、高磁場下ホール抵抗率測定により移動度及びキャリア密度の評価を行った。

実験結果

面直、面内 X 線回折測定から基板温度(T_S)= 300～600℃の範囲において MCA が基板に対して 45°回転してエピタキシャル成長していることが確認できた(MCA (001)[110] // MgO or MAO (001)[100]) (Fig. 1)。また、磁化測定によって室温で強磁性体又はフェリ磁性体に特有のヒステリシス曲線を観測した(Fig.2)。アシストガンを用いた低温製膜によって T_S の減少と共に格子定数(c)と飽和磁化(M_S)が増大し、T_S = 300 ℃で c = 0.5792 nm , M_S = 235 emu/cc となり、バルク値(0.5798 nm , 350 emu/cc)と同等の値となった。これらは低温製膜によって界面反応やミキシング、Mn 原子の欠損などが抑制されたためであると考えられる。さらに、電気抵抗測定から、温度低下に伴って抵抗値が増大するという半導体的な挙動が確認された。アレニウスプロットによって求めた活性化エネルギーは数 meV 程度と非常に小さな値が得られ、SGS がゼロギャップ半導体であることに対応していると考えられる。また、4 K でのホール抵抗率測定によって得られた電子移動度及びキャリア密度はそれぞれ 17 $cm^2/V\cdot s$, 5×10^{20} cm^{-3} であり、薄膜において報告されている値(0.45 $cm^2/V\cdot s$, 1.6×10^{20} cm^{-3})[2]より 2 桁大きな移動度が得られた。これは原子置換や欠損がより少ないためだと考えられる。

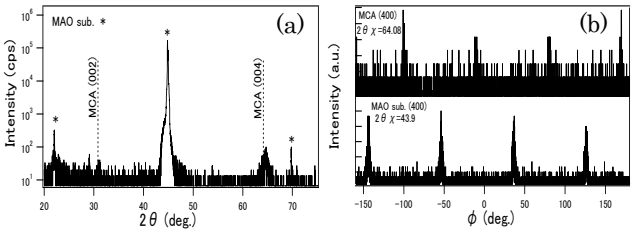

Fig. 1 (a) Out-of-plane, (b) in-plane XRD patterns for MCA films on MAO formed at 350℃

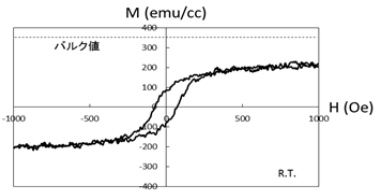

Fig. 2 Magnetic field dependence of Magnetization curves of MCA films on MAO formed at 300℃

参考文献

1) M. Nishiwaki et. al., J. Appl. Phys., 117, 17D719 (2015).
2) Xu, et. al., Appl. Phys. Lett., 104, 242408 (2014).

Fe_4N エピタキシャル薄膜の窒素原子占有度の評価

伊藤啓太[1,2,3]，具志俊希[1]，東小薗創真[1]，竹田幸治[4]，斎藤祐児[4]，都甲薫[1]，柳原英人[1]，
角田匡清[2]，小口多美夫[5]，木村昭夫[6]，喜多英治[1]，末益崇[1]
([1]筑波大，[2]東北大，[3]日本学術振興会 PD，[4]日本原子力研究開発機構，[5]大阪大，[6]広島大)

Characterization of occupancy of nitrogen atoms in epitaxially grown Fe_4N films

K. Ito[1,2,3], T. Gushi[1], S. Higashikozono[1], Y. Takeda[4], Y. Saitoh[4], K. Toko[1], H. Yanagihara[1],
M. Tsunoda[2], T. Oguchi[5], A. Kimura[6], E. Kita[1], and T. Suemasu[1]
([1]Univ. of Tsukuba, [2]Tohoku Univ., [3]JSPS, [4]JAEA, [5]Osaka Univ., [6]Hiroshima Univ.)

はじめに

逆ペロブスカイト型遷移金属強磁性窒化物(Fig. 1)は近年スピントロニクス応用材料として注目を浴びている。特に Fe_4N は、スピン依存電気伝導度計算から大きな負のスピン分極率(P_σ = −1.0)が予想されている[1]。我々はこれまでに分子線エピタキシー(MBE)法により、$SrTiO_3$(STO)(001)基板上へのエピタキシャル膜の作製に成功している[2]。一方、N 原子の占有度はスピン分極率に影響すると考えられ、それを調べる事は応用上の観点からも重要である。これまで X 線回折(XRD)法を用いた評価結果が報告されているが[3]、平均的な情報を取り扱うため、詳細な情報は得られていなかった。そこで本研究では、MBE 法により Fe_4N 薄膜をエピタキシャル成長し、内部転換電子メスバウアー(CEMS)測定、X 線吸収分光(XAS)、X 線磁気円二色性(XMCD)測定を行い、XRD 法ではわからない局所的な情報が得られる、新たな Fe_4N 中の N 原子の占有度評価手法の提案を試みた。

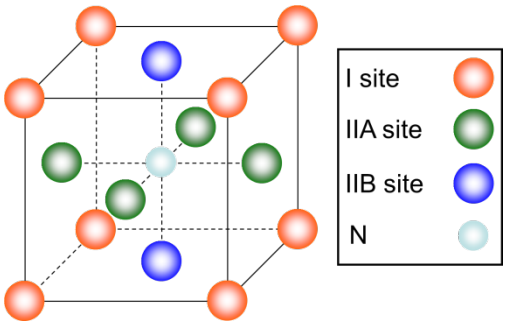

Fig. 1 Lattice of anti-perovskite nitride.

実験方法

固体 Fe と高周波プラズマ N_2 の同時供給による MBE 法により、STO(001)基板上に Fe_4N(20 nm)をエピタキシャル成長し、300 K にて CEMS 測定を行った。Fe 原料は ^{57}Fe の割合を 20%程度にエンリッチした特殊原料を用いた。XAS および XMCD 測定には Au(3 nm)/Fe_4N(10 nm)を用いた。300 K にて試料の面直方向に±3 T の磁場を印加し、飽和状態で測定した。全電子 FLAPW 法に基づく第一原理電子状態計算の結果とフェルミの黄金則を用いて XAS および XMCD スペクトルを計算し、実験結果と比較した。

実験結果

理想的には各 Fe site の占有比率は Fe I:Fe II = 1:3 だが、CEMS スペクトルの解析結果は Fe I:Fe II = 0.53:3 となった。理想と異なり N 原子が隣り合う 2 つの Fe I site 間に侵入した場合、Fe I site が Fe II site と等価になる。よって、N 原子の過剰侵入または不規則占有に起因して、Fe I site の見かけの占有比率が小さくなったと考えられる[4]。XAS および XMCD スペクトルの Fe $L_{2,3}$ 吸収端には肩構造が現れ、理論計算からも再現された。この肩構造は、Fe II site の Fe 3*d* 軌道と N 2*p* 軌道との混成に起因した局所的な電子状態を反映したものであり[5]、N 原子の侵入量や規則度との関連性が高いといえる。

謝辞
本研究は JSPS 科研費(No. 26249037)、特別研究員奨励費(No. 14J01804)の支援を受けた。CEMS 測定は、筑波大学研究基盤総合センター応用加速器部門にて行った。XAS および XMCD 測定は、ナノネット支援課題(Nos. 2010A3877 and 2010B3876)のもと、SPring-8 BL23SU にて行った。

参考文献

1) S. Kokado *et al.*, Phys. Rev. B **73**, 172410 (2006). 2) K. Ito *et al.*, J. Cryst. Growth **322**, 63 (2011). 3) K. Kabara *et al.*, Appl. Phys. Express, **7**, 063003 (2014). 4) K. Ito *et al.*, J. Appl. Phys. **117**, 17B717 (2015). 5) K. Ito *et al.*, J. Appl. Phys. **117**, 183906 (2015).

Mapping of theoretical approach in magnetics

– coarse graining theory–

Chiharu Mitsumata
(NIMS)

Nowadays, the objects for magnetics are spreading to various fields. Under those circumstance, the requirements to theoretical analysis increase, i.e. a simple modeling, numerical prediction, etc. Besides, the requests such as materials predictions based on the data base analysis called “materials informatics” or “material genome” become strong, too.

Generally, from a viewpoint of magnetics, it is necessary to understand the magnetization distribution and/or a magnetization process in devices and materials. In this sense, the micromagnetics theory is convenient to understand the side view of the phenomenalism. However, that theory is insufficient to define the exact property, because it does not include self-consistency of theory. To obtain the accurate magnetic property, the knowledge from a microscopic theory should be required.

For the discussion of magnetization state, the magnetic energy can be defined by following procedure,

1) Spin–spin interaction (including the exchange interaction, spin transfer) is evaluated within a framework of electric theory.
2) The magnetic anisotropy constant is evaluated within a framework of first principles calculation for certain materials.
3) The magnetic dipole interaction is generally evaluated by the numerical calculation of a classical spin model.
4) The thermo-dynamic behavior of magnetization is evaluated by the statistical average of a classical spin model.

Then, the obtained magnetic energies reflect onto the micromagnetics calculation. At this point, the atomistic calculation is ready to carry out.

However, to analyze the entire body of materials and devices, the atomistic calculation needs to expend too much computational resources. In this sense, it is required well defined coarse graining theory for connecting atomistic calculations and conventional micromagnetics calculations.

In terms of energy evaluation 3), the multipole expansion method naturally deals with the magnetic dipole interaction, in which the contribution from the distant part is averaged over a certain volume. For 4), the formulation of the Landau-Lifshitz-Bloch equation is suggested[1)], which includes the degree of freedom for permitting the expansion and

contraction of the magnetization vector. For 1), the method of single spin approximation[2)] is one of the candidate to deal with the exchange interaction between the textured grains. Finally, for 2), the conversion from a single site anisotropy to the expression of energy density form simply satisfies the coarse graining.

Reference

1) D. A. Garanin: "Fokker-Planck and Landau-Lifshitz-Bloch equations for classical ferromagnets", *Phys. Rev. B*, **55**, 3050 (1997)

2) S.-J. Lee, S. Sato, H. Yanagihara, E. Kita, C. Mitsumata: "Numerical simulation of random magnetic anisotropy with solid magnetization grains", *J. Magn. Magn. Mater.*, **323**, 28 (2011)

Fundamental knowledge of first-principles calculation

M. Shirai
Research Institute of Electrical Communication, Tohoku University, Sendai 980-8577, Japan

In this tutorial talk, the fundamentals of first-principles calculation are briefly reviewed for beginners. The theoretical framework of first-principles calculation, i.e. so-called density-functional theory was established by Hohenberg and Kohn[1]. They probed that the ground-state energy of an inhomogeneous electron gas can be expressed as a functional of the electron density $n(\boldsymbol{r})$ and the energy functional takes its minimum value for the correct ground-state. The advantage of the theory is that we need no explicit expression for the wave function of an interacting electron system. The density-functional theory gives us a firm base for understanding the complex interacting electron systems. However, no one knows an explicit expression of the energy functional. A practical method treating an interacting electron system was proposed by Kohn and Sham[2] on the basis of the density-functional theory. They reduced the many-body problem of interacting electron systems to self-consistent equations, i.e. Kohn-Sham equations, for single electron in an effective potential, which contains exchange and correlation terms. They assumed that the exchange and correlation potentials depend only on the electron density at the position where the potential is acting. We usually adopt the explicit form of the exchange and correlation potentials for a homogeneous electron gas. This is called local density approximation (LDA). The treatment enables us to obtain the ground state energy as well as the energy band-structure of complex systems such as molecules and solids. However, there are drawbacks originated from the LDA; overestimation of cohesive energy and hence underestimation of inter-atomic distances, underestimation of band gap of semiconductors or insulators including Mott-Hubbard insulators caused by electron correlation effect, underestimation of exchange splitting of spin-up and down bands in magnetic materials, and so on. Some of these drawbacks can be overcome by improved treatments of the exchange and correlation potentials; i.e. generalized gradient approximation[3], self-interaction correction[4], LDA+U method[5], self-energy correction including GW approximation[6] and dynamical mean-field approximation[7], and so on. Typical examples calculated with use of these approaches are presented and the shortcoming of them will be discussed.

Reference
1) P. Hohenberg and W. Kohn, Phys. Rev. **136** (1964) B864.
2) W. Kohn and L. J. Sham, Phys. Rev. **140** (1965) A1133.
3) J. P. Perdew and Y. Wnag, Phys. Rev. B **33** (1986) 8800.
4) J. P. Perdew and A. Zunger, Phys. Rev. B **23** (1981) 5048.
5) V. I. Anisimov, J. Zaanen, and O. K. Andersen, Phys. Rev. B **44** (1991) 943.
6) L. Hedin, Phys. Rev. **139** (1965) A796.
7) A. Georges and G. Kotliar, Phys. Rev. B **45** (1992) 6479.

磁化構造中の伝導電子の理論

多々良源
(理化学研究所創発物性科学研究センター (CEMS))

Theory of electron transport in the presence of magnetization textures

G. Tatara
RIKEN Center for Emergent Matter Science (CEMS)

1　Introduction

In this paper, we discuss two topics, an emergent electromagnetic field which couples to electron's spin in ferromagnetic metals [1] and current-induced torques [2] from the theoretical viewpoints.

Our technology is based on various electromagnetic phenomena. For designing electronics devices, thus, the Maxwell's equation is of essential importance. The mathematical structure of the electromagnetic field is governed by a U(1) gauge symmetry, i.e., an invariance of physical laws under phase transformations. The gauge symmetry is equivalent to the conservation of the electric charge, and was established when a symmetry breaking of unified force occured immediately after the big bang. The beautiful mathematical structure of charge electromagnetism was therefore determined when our universe started, and there is no way to modify its laws.

Fortunately, charge electromagnetism is not the only electromagnetism allowed in the nature. In fact, electromagnetism arises whenever there is a U(1) gauge symmetry associated with conservation of some effective charge. In solids, there are several systems which have the U(1) gauge symmetry as a good approximation. Solids could thus display several types of effective electromagnetic fields. A typical example is a ferromagnetic metal. In ferromagnetic metals, conduction electron spin (mostly s electron) is coupled to the magnetization (or localized spins of d electrons) by an interaction called the sd interaction, which tends to align the electron spin parallel (or anti-parallel) to the localized spin. This interaction is strong in most $3d$ ferromagnetic metals, and as a result, conduction electron's spin originally consisting of three components, reduces to a single component along the localized spin direction. The remaining component is invariant under a phase transformation, i.e., has a U(1) gauge symmetry just like the electric charge does. A spin electromagnetic field thus emerges that couples to conduction electron's spin. The first subject of the present paper is this spin electromagnetic field. The world of spin electromagnetic field is richer than that of electric charge, since the electron's spin in solids is under influence of various interactions such as spin-orbit interaction. We will in fact show that magnetic monopole emerges from spin relaxation processes. Spin electromagnetic field drives electron's spin, and thus plays an essential role in spintronics. The other subject, the current-induced torques, is a reciprocal effect of spin electromagnetic field.

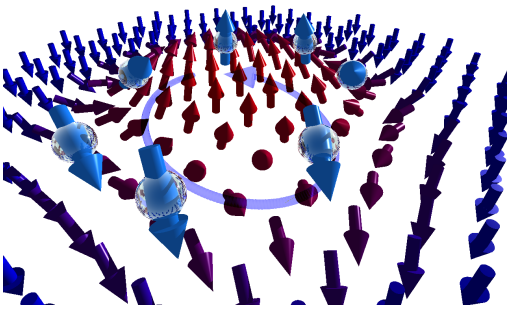

Fig. 1　The spin of a conduction electron is rotated by a strong sd interaction with magnetization as it moves in the presence of a magnetization texture, resulting in a Berry's phase factor $e^{i\varphi}$

The effect of spin electromagnetic field was partially discussed already in 1986 by Berger, who discussed a voltage generated by a canting of wall plane of a driven domain wall [3]. Emergence of effective electromagnetism coupling to electron's spin was pointed out by use of gauge field argument by Volovik in 1987 (Ref. [4]). Stern discussed the motive force in the context of the spin Berry's phase, and discussed similarity to the Faraday's law [5]. Spin motive force was rederived in Ref. [6] in the case of domain wall motion. It was argued in the context of topological pumping in Ref. [7]. Duine discussed spin electric field including the effect of spin relaxation by use of non-adiabaticity parameter (β) [8,9]. The Hall current induced by a spin electric field in the presence of spin-orbit interaction was theoretically studied by Shibata and Kohno [10,11]. The effect of Rashba

interaction on spin electric field was discussed in Refs. [12,13]. These works [6,8,10,12,13] have focused solely on the spin electric field. The magnetic component of Rashba-induced spin electromagnetic was discussed in Ref. [14].

2 Emergence of spin gauge field

Let us here demonstrate that a spin gauge field emerges from a strong *sd* exchange interaction (adiabatic limit). Because of the *sd* interaction, spin of electron traveling through a magnetization structure follows the local spin and rotates with it (Fig. 1), and the spin acquires a geometric phase [15]. The phase is written as an integral of an effective gauge field, $\boldsymbol{A}_{\rm s}$, along its path C as $\varphi = \frac{e}{\hbar}\int_C d\boldsymbol{r}\cdot\boldsymbol{A}_{\rm s}$, where e is electron charge and $\hbar$ is the Planck's constant devided by 2π. The vector $\boldsymbol{A}_{\rm s}$ turns out to be

$$\boldsymbol{A}_{\rm s} = \frac{\hbar}{2e}(1-\cos\theta)\nabla\phi. \tag{1}$$

Existence of the phase means that there is an effective magnetic field, $\boldsymbol{B}_{\rm s}$, as seen by rewriting the integral over a closed path using the Stokes theorem $\varphi = \frac{e}{\hbar}\int_S d\boldsymbol{S}\cdot\boldsymbol{B}_{\rm s}$, where $\boldsymbol{B}_{\rm s} \equiv \nabla\times\boldsymbol{A}_{\rm s}$ represents curvature. This phase φ attached to electron spin is called the spin Berry's phase. Time-derivative of phase is equivalent to a voltage, and thus we have effective electric field defined by $\dot{\varphi} = -\frac{e}{\hbar}\int_C d\boldsymbol{r}\cdot\boldsymbol{E}_{\rm s}$, where $\boldsymbol{E}_{\rm s} \equiv -\dot{\boldsymbol{A}}_{\rm s}$. $\boldsymbol{E}_{\rm s}$ and $\boldsymbol{B}_{\rm s}$ are called spin electric and magnetic field, respectively. They satisfy the Faraday's law,

$$\nabla\times\boldsymbol{E}_{\rm s} + \dot{\boldsymbol{B}}_{\rm s} = 0, \tag{2}$$

as a trivial result of their definitions. The fields have a structure of electromagnetism and thus a spin electromagnetic field coupled to electron's spin emerges. One should note that those fields are real or observable ones coupling to real electric charge and current and not just 'fictitious fields'.

In the presentation, phenomena arising from the spin gauge field, Eq. (1), are discussed.

References

1) G. Tatara and N. Nakabayashi. Emergent spin electromagnetism induced by magnetization textures in the presence of spin-orbit interaction (invited). *Journal of Applied Physics*, Vol. 115, No. 17, p. 172609, 2014.

2) G. Tatara, H. Kohno, and J. Shibata. Microscopic approach to current-driven domain wall dynamics. *Physics Reports*, Vol. 468, pp. 213–301, 2008.

3) L. Berger. Possible existence of a josephson effect in ferromagnets. *Phys. Rev. B*, Vol. 33, No. 3, pp. 1572–1578, 1986.

4) G. E. Volovik. Linear momentum in ferromagnets. *J. Phys. C: Solid State Phys.*, Vol. 20, pp. L83–L87, 1987.

5) A. Stern. Berry's phase, motive forces, and mesoscopic conductivity. *Phys. Rev. Lett.*, Vol. 68, No. 7, pp. 1022–1025, Feb 1992.

6) S. E. Barnes and S. Maekawa. Generalization of faraday's law to include nonconservative spin forces. *Phys. Rev. Lett.*, Vol. 98, No. 24, p. 246601, 2007.

7) S. A. Yang, G. S. D. Beach, C. Knutson, D. Xiao, Z. Zhang, M. Tsoi, Q. Niu, A. H. MacDonald, and J. L. Erskine. Topological electromotive force from domain-wall dynamics in a ferromagnet. *Phys. Rev. B*, Vol. 82, p. 054410, Aug 2010.

8) R. A. Duine. Spin pumping by a field-driven domain wall. *Phys. Rev. B*, Vol. 77, No. 1, p. 014409, 2008.

9) M. E. Lucassen, G. C. F. L. Kruis, R. Lavrijsen, H. J. M. Swagten, B. Koopmans, and R. A. Duine. Spin motive forces due to magnetic vortices and domain walls. *Phys. Rev. B*, Vol. 84, p. 014414, Jul 2011.

10) J. Shibata and H. Kohno. Inverse spin hall effect driven by spin motive force. *Phys. Rev. Lett.*, Vol. 102, No. 8, p. 086603, 2009.

11) J. Shibata and H. Kohno. Spin and charge transport induced by gauge fields in a ferromagnet. *Phys. Rev. B*, Vol. 84, p. 184408, Nov 2011.

12) K.-W. Kim, J.-H. Moon, K.-J. Lee, and H.-W. Lee. Prediction of giant spin motive force due to rashba spin-orbit coupling. *Phys. Rev. Lett.*, Vol. 108, p. 217202, May 2012.

13) G. Tatara, N. Nakabayashi, and K.-J. Lee. Spin motive force induced by rashba interaction in the strong *sd* coupling regime. *Phys. Rev. B*, Vol. 87, p. 054403, Feb 2013.

14) N. Nakabayashi and G. Tatara. Rashba-induced spin electromagnetic fields in the strong sd coupling regime. *New Journal of Physics*, Vol. 16, No. 1, p. 015016, 2014.

15) J. J. Sakurai. *Modern Quantum Mechanics*. Addison Wesley, 1994.

Numerical methods for quantum magnets

Seiji MIYASHITA
(Department of Physics, Graduate School of Science, The University of Tokyo)

Methods for studies on quantum magnets are overviewed. In the classical picture, spin can be regarded as a vector of magnetic moment. But, various interesting properties due to the quantum effects have been studied as the so-called 'quantum spin systems'[1]. Quantum mechanical effect in spin systems is originated in the non-commutative property of spin operators: $[S_x, S_y] = i\hbar S_z$, etc. In order to take into account the quantum effect, we need to treat the Hamiltonian matrix $\mathcal{H}$ of the system whose matrix is of 2^Nx2^N for a system consisting of N spins of S=1/2. The straightest way to study the system is a diagonalization method to obtain the eigenvalues and eigenvectors of the matrix. To study finite temperature properties, we calculate Tr exp(-β$\mathcal{H}$), and we need all the eigenvalues and eigenvectors[2]. However, often we are interested in low temperature properties of the system, in particular the ground system. There, we may use iterative methods for the low energy states, such as the Lanczos method. For such purpose, TIT-pack was released[3], which encouraged studies in this field in Japan, and several method to extrapolate the data has been developed.[4]. But, the system size is still limited.

To study a large system a quantum Monte Carlo (QMC) method by making use of the Suzuki-Trotter method[5] has been introduced. This method has been developed with the idea of the loop algorithm and the continuous imaginary time algorithm[6], and methods to take into account effects of lattice distortion have been also developed. Now QMC is the one of the most reliable methods for quantum many body systems. However, the method consists of a sampling of the so called world lines (paths in the path-integral method) [7], and suffers from the so-called 'negative sign' problem, and cannot be applied to frustrated system efficiently.

As an efficient method to study large systems in one dimension (1D), the so-called DMRG (density matrix renormalization group) method was invented[8]. The idea of this method has been developed and is now one of the most powerful method for 1D systems. This method is extended to higher dimensions[9] also to finite temperatures. The similar idea has been introduced as the matrix-product method[10], and recently it has been studied extensively as tensor-network methods.[11]

Magnetic resonance is also an important subject of the study of magnetism. The ESR spectrum is given by Kubo formula. As a microscopic approach, a direct calculation of the formula by making use of full diagonalization has been introduced[12], which gives precise information of the spectrum for given systems, e.g., the effect of spatial configuration of the lattice, the dependence on the field direction. Application of this method is also limited to small sizes because it uses diagonalization of the system Hamiltonian. For the ESR spectrum in the ground state, we may use the idea of Lanczos method, and also DMRG (dynamical DMRG)[13,14]. For finite temperatures we can make use of the time evolution of the so-called typical state.[15,16,17] The field and temperature dependent in 1D systems has been studied bay making use of field theoretical informations[18]. The typical state would give a seminal method to give temperature dependent thermal properties[17].

Moreover quantum dynamics is also an important issue in quantum magnets. The dynamics of magnetization under time dependent field reflects the energy level structure of the system. Such effect was observed in single molecular magnets (SMM) such as Mn12, Fe8, and V15, etc. [19] The importance of the Landau-Zener process was pointed out.[20] The dynamics in dissipative environments is treated by the quantum master equation[21]. The combination of quantum dynamics and dissipative effects provides interesting phenomena, such as the phonon-bottleneck effect or magnetic Foehn effect[22]. Recently the hybridization between magnetic state and photon state in a cavity attracts interests in the context of manipulation of quantum state. The quantum master equation is also used to emulate such quantum dynamics[23]. In quantum systems, the so-called quantum fluctuation plays an important role. By making this fact, the so-called quantum annealing method was invented[24]. This method is used in a quantum computing of the D-wave machine.[25]

With the development of super-computer such as the K-computer, massive parallel algorithm allows us to use a large

memory. Such technique has been established, and now systems with more than 40 spins (S=1/2), can be calculated.[26] Recently the system ALPS is released for non-specialists, in which some of the above methods are prepared in user-friendly way[27].

Reference

1) S. Miyashita: 量子スピン系 (in Japanese), Iwanami-Shoten (2006).
2) J. Oitmaa and D. D. Betts: Can. J. Phys. **56** (1978) 897.
3) TITPACK: http://www.stat.phys.titech.ac.jp/~nishimori/titpack2_new/index-e.html
4) 野村清英，岡本清美: BKT 転移とレベルスペクトロスコピー，日本物理学会誌 **56** (2001) No.11, pp.836-844. K. Okamoto, T. Tonegawa, H. Nakano, T. Sakai, K. Nomura and M. Kaburagi: J. Phys. Conf. Ser. **320** (2011) 012018.
5) M. Suzuki: Prog. Theor. Phys. **56** (1976) 1454. M. Suzuki, S. Miyashita and A. Kuroda: Prog. Thoer. Phys. **58**, 1377-1387 (1977). *Quantum Monte Carlo method in Equilibrium and Nonequilibrium Systems*, ed. M. Suzuki (springer-Verlag, 1987).
6) H. G. Evertz: Adv. Phys. **52** (2003) 1.
7) H. Onishi and S. Miyashita: J. Phys. Soc. Jpn. **72**, 392 (2003).
H. Sawa, *Geometrically Constructed Markov Chain Monte Carlo Study of Quantum Spin-phonon Complex Systems,* Springer (2014) DOI 10.1007/978-4-431-54517-0.
8) S. R. White: Phys. Rev. Lett. **69** (1992) 2863; Phys. Rev. B **48** (1993)10345.U. Schollwock, Rev. Modern Phys. **77** (2005) 259; and Ann. Phys. **326** (2011) 96. 西野友年、日永田泰啓、奥西巧一: 日本物理学会誌 **55** (2000) 763.
9) T. Nishino, Y. Hieida, K. Okunishi, N. Maeshima, Y. Akutsu, A. Gendiar, Prog. Theor. Phys. 105 (2001) 409.
10) G. Vidal, Phys. Rev. Lett. **91** (2003) 147902, and ibid. **93** (2004) 040502.
A.J. Daley, C. Kollath, U. Schollwock, G. Vidal, J. Stat. Mech.: Theor. Exp. (2004) P04005. S.R. White, A.E. Feiguin, Phys. Rev. Lett. **93** (2004) 076401.
11) R. Oris: Ann. Phys. **349** (2014) 117.
12) S. Miyashita, T. Yoshino and A. Ogasahara, J. Phys. Soc. Jpn. **68**, 655 (1999).
13) S. Ramasesha, S. K. Pati, H. R. Krishnamurthy, Z. Shuai, and J. L. Br´edas, Phys. Rev. B 54, 7598 (1996). E. R. Gagliano and C. A. Balseiro, Phys. Rev. Lett. **59**, 2999 (1987).,.
14) E. Jeckelmann: Phys. Rev. B **66**, 045114 (2002).
15) T. Iitaka and T. Ebisuzaki, Phys. Rev. Lett. **90**, 047203 (2003). M. Machida, T. Iitaka, and S. Miyashita, Phys. Rev. B **86**, 224412 (2012)
16) A. Hams and H. De Raedt, Phys. Rev. E **62**, 4365 (2000)
17) S. Sugiura and A. Shimizu, Phys. Rev. Lett. **108**, 240401 (2012).
18) M. Oshikawa and I. Affleck, Phys. Rev. B **65**, 134410 (2002).
19) B. Barbara, Phil. Trans. R. Soc. A **370**, 4487 (2012). L. Thomas, et al., Nature **383**, 145 (1996). C. Sangregorio, et al., Phys. Rev. Lett. **78**, 4645 (1997).
20) L. D. Landau, Phys. Z. Sowjetunion **2**, 46 (1932); C.Zener, Proc. R. Soc. London, Ser. A **137**, 696 (1932);E. C. G. Stuekelberg, Helv. Phys. Acta **5**, 369 (1932); E. Majorana, Nuovo Cimento **9**, 43 (1932). S. Miyashita, J. Phys. Soc. Jpn. **64**, 3207 (1995); ibid. **65**, 2734 (1996). 宮下精二:日本物理学会誌 **53** (1998) 259.
21) K. Saito, S. Miyashita and H. De Raedt: Phys. Rev. B **60** (1999)14553.
斉藤圭司、宮下精二:日本物理学会誌 **59** (2004) 760.
22) I. Chiorescu, W. Wernsdorfer, A. Mu¨ller, H. Bo¨gge and B.Barbara: Phys. Rev. Lett. **84** (2000) 3454. K. Saito and S. Miyashita: J. Phys. Soc. Jpn. **70**, 3385-3390 (2001).
23) I. Chiorescu, N. Groll, S. Bertaina, T. Mori and S. Miyashita: Phys. Rev. B **82**, 024413 (2010).
S. Miyashita, T. Shirai, T. Mori, H. De Raedt, S. Bertaina, I. Chiorescu: J. Phys. B **45**, 124010 (2012).
24) T. Kadowaki and H. Nishimori, Physical Review E, Vol. **58**, 5355 (1998). A. Das and B. K. Chakrabarti, Reviews of Modern Physics, **80**, 1061(2008). G. Santoro and E. Tosatti, Journal of Physics A, **39**, R393 (2006).
大関真之、西森秀稔:日本物理学会誌 Vol. **66**, p. 25, (2011).
25) H. Nishimori: http://www.stat.phys.titech.ac.jp/nishimori/
26) H. Nakano and T. Sakai: J. Phys. Soc. of Jpn. **83** 104710 (2014).
27) B. Bauer et al. J. Stat. Phys. (2011) P05001. 藤堂眞治: 日本物理学会誌 **70** (2015) 275.

Micromagnetic Simulation

Y. Nakatani
(University of Electro-Communications, Chofu 182-8585,Japan)

Since the pioneering works by Brown and LaBonte[1-3], micromagnetic simulation has been used to calculate the magnetization distribution and its dynamics in nanoscale magnetic materials. Because of the limitations of the calculation speed of the computers, they proposed the simple algorithms to obtain the energy minimum state, and solved the problem within these limitations[1-6]. Usually, the exchange, anisotropy, Zeeman, and the demagnetizing energies are considered in micromagnetic simulation.

$$\varepsilon = A(\nabla \mathbf{m})^2 + K_u \sin^2\theta - \frac{1}{2}\mathbf{H}^D \cdot \mathbf{m} - \mathbf{H}^E \cdot \mathbf{m}. \qquad (1)$$

Here, A, K_u, $\boldsymbol{H^D}$ and $\boldsymbol{H^E}$ are the exchange stiffness constant, the uniaxial anisotropy constant, the demagnetizing field and the external field, respectively.

In 1980s, third generation supercomputers appeared and they extended the limitations. Micromagnetic simulation was used to solve some problems, i.e., the magnetic domain wall dynamics[7,8], magnetic fine particle[9,10], magnetic thin film[11], magnetic recording media[12], and magneto-optical recording media[13]. In these reports, Landau-Lifshitz-Gilbert equation was used.

$$\dot{\mathbf{m}} = -\gamma \mathbf{m} \times \mathbf{H} - \frac{\alpha}{M_s}\dot{\mathbf{m}} \times \mathbf{m}. \qquad (2)$$

$$\rightarrow \dot{\mathbf{m}} = -\frac{\gamma}{1+\alpha^2}\left[\mathbf{m} \times \mathbf{H} + \alpha\left[\mathbf{m} \times (\mathbf{m} \times \mathbf{H})\right]\right]. \qquad (3)$$

$$\mathbf{H} = -\frac{\delta \varepsilon}{\delta \mathbf{m}}. \qquad (4)$$

Here $\boldsymbol{H}$ is the effective field acting on the magnetic moments. It is calculated by using eq. (4). However since the calculations of the demagnetizing field required a lot of calculation time even with the supercomputers[14,15], they could not solve the LLG equation with original form in many cases. However in these cases, they only needed the switching field of magnetic fine particles or thin films, and did not need the dynamics of the magnetic moments. In the cases, they dropped the gyroscopic term from the LLG equation (eq.(5)), and used a unity of the Gilbert damping constant to reduce the calculation time [9-12].

$$\dot{\mathbf{m}} = -\frac{\gamma}{1+\alpha^2}\left[\alpha\left[\mathbf{m} \times (\mathbf{m} \times \mathbf{H})\right]\right] \qquad (5)$$

In 1990s, the fast Fourier transform (FFT) algorithms were introduced to calculate the demagnetizing field[19,20]. It reduced the calculation time drastically. By using this algorithm, the LLG equation with original form can be solved, and larger scale and longer time simulation can be done with personal computers. Nowadays, there are many open source programs and products for micromagnetic simulation[21], micromagnetic simulation is used in many fields, such as nanospintronics, permanent magnet, etc, not only to analyze the experimental results, but also to obtain the optimum conditions of nanodevices. Recently, many effects except for in eq. (1) are discussing, such as Rashba field effect, spin hall effect, Dzyaloshinsky-Moriya interaction, etc. These effects can be adapted to the simulation as the effective field. However even with the personal computers in recent years, the size of the simulation region, which can be simulated within the acceptable time, is about ～0.5 μ m^2 in 2D model case. For larger scale or long time simulations, special computers such as GPU or massively parallel computers are required[22].

For the experimentalist, one of the interested points for the simulation is comparison of the simulation and experimental results. In case of the simple structure target, such as a single crystal material, simulation results in good agreement with the experimental results without special modification of the simulation model. However in case of the complex structure target, such as polycrystalline material, many modifications of the simulation model are required. In the presentation, the simulation results in these two cases will be presented[23-24]. The important points for the simulation will be also presented.

Reference

1) W. F. Brown and A. E. Labonte, *J. Appl. Phys.*, **36**, 1380 (1965).
2) A. E. LaBonte, and W. F. Brown, Jr., JAP, 37, 3, 1299 (1966).
3) A. E. LaBonte, JAP, 40, 6, 2450 (1969).
4) A. Hubert, Phys. Stat. Solidi, 32, 519 (1969).
5) A. Hubert, Phys. Stat. Solidi, 38, 699 (1970).
6) A.Hubert, *IEEE Trans on Magn.* MAG-11, 1285 (1975).
7) C.C. Shir, *JAP*, 49, 3413 (1978).
8) Y. Nakatani, et. al., *IEEE Trans on Magn.* MAG-23, 2179 (1987).
9) E. Della Torre, *IEEE Trans on Magn*. MAG-21, 1423 (1985).
10) D. R. Fredkin, et. al., *IEEE Trans on Magn*., MAG-23, 3385 (1987).
11) R. H. Victora, *PRL*, 58, 1788 (1987).
12) J.-G. Zhu, et. al., *IEEE Trans on Magn*. MAG-24, 2706 (1988).
13) M. Mansuripur, et. al., *JAP*, 63, 3831 (1988)
14) M. E. Schebes and A. Aharoni, IEEE Trans. Magn., MAG-23, 3882 (1987).
15) H. Fukushima, Y. Nakatani, N. Hayashi, IEEE Trans. Magn., MAG-34, Jan,1998, pp.193-198.
16) M. Mansuripur and R. Giles, *IEEE, Trans*. Mag-24, 2326 (1988).
17) A. Thiaville, et. al., *JAP*, 69, 6090 (1991).
18) L. Greengard and V. Rokhlin, *J. Comp. Phys.*, 135, 280 (1997).
19) S. W. Yuan, et. al., *IEEE Trans. Magn.*, **28**, 2031 (1992).
20) N. Hayashi, et. al., Jpn, J. Appl. Phys, **35**, 6065 (1996).
21) http://deparkes.co.uk/2014/05/30/list-micromagnetic-simulation-software/
22) M. Tate, et. al., *Dig. INTERMAG 2009*, Sacrament, AS-10 (2009).
23) A. Thiaville, et. al., *J. Appl. Phys*., **69**, 6090 (1991).
24) Y. Nakatani, et. al., *Nature Mat*., **2**, 521 (2003).

Finite Element Analysis for Electromechanical Design

Takashi Yamada[1]
[1] JSOL Corporation, Tokyo 104-0053, Japan

Finite Element Analysis (FEA) is indispensable to design and development of electromagnetic field applications in industry as well as academic and several software packages for FEA are commercially available today. The basics of ElectroMagnetic (EM) FEA, use cases and future work will be explained here. It should be noted that electromagnetic applications can be classified into two categories, i.e. High Frequency (HF) and Low Frequency (LF) and this explanation will focus on the LF. Although the names imply that there exists a frequency as the divider, no such a clear boundary frequency exists since the divider is significance of the displacement current in the application's phenomena. Typical applications of HF are antennas, microstriplines and waveguides. LF, on the other hand, has motors, transformers and sensors, in which the magnetic field is dominant over the electric field.

The EM FEA was started in late of 1970 in the electrical engineering by utilizing the structural FEA technology which was originally developed for computational vibration analysis for aircraft in late 1960[1)]. The applications in the early stage were power transformers and generators[2)] for both of which prototyping is difficult due to the size and sophisticated design is required to achieve high efficiency and reliability for power supply in social infrastructure. Those successes expanded its application range to other systems and products such as TV tubes[3)4)], solenoid valves[5)], magnetic recording heads[6)], EM shields[7)], induction heating systems[8)], non-destructive testing[9)]. In the mid of 1990, as well known as Kyoto Protocol, the energy efficiency improvement became a must time in most electrical applications such air-conditioners[10)] and electric vehicles (EV)[11)] and hybrid vehicles (HV)[12)13)] which have to have very high efficient motors. To achieve the super high efficiency, the FEA was heavily used and it is still going on today.

The basic equation of the EM FEA is the Maxwell's equations with two constitutive equations which represent material characteristics and the displacement current term is omitted from them for LF. This modification decouples electric field from magnetic field so that it becomes easier to solve three equations rather than all the four equations. The drawback is, of course, one cannot see electric field effects such as displacement current flowing in a capacitor.

It does not mean LF is easier than HF in which one has to solve the four equations because, in LF, there exists magnetic saturation that leads to the non-linear problem and many applications have motion which is difficult to handle for EM where both space and objects are have to be modeled.

The remaining three equations can be unified by introducing magnetic vector potential instead of handling magnetic field directly.

The unified equation is transformed by Finite Element Method (FEM) into a form which can be solved by computers. In FEM, an analysis region, which includes magnetic materials, conductors and spaces, and time are discretized into small elements and time intervals. The union of elements is called mesh. The field value, which is magnetic vector potential in this case, is represented with a polynomial using interpolation functions. It means that the accuracy of the solution depends on the discretization, that is that smaller elements and time interval will give more accuracy.

The resulting discretized equation forms a matrix equation in which the coefficient matrix contains material characteristics and the load vector contains currents/voltage/permanent magnet. It is solved by a linear equation solver to obtain the magnetic vector potential. Recalling that the magnetic materials usually have complex behavior such as magnetic saturation and hysteresis characteristics, the equation is basically non-linear and needs to be solved with iterative manner. It should be noted that the dimension of the matrix increases as the number of the elements increases so that efficient meshing techniques is important to generate efficient meshes which have enough elements only for sensitive regions minimizing the total number of elements. After obtaining the magnetic vector potential, several physical quantities are naturally derived, such as magnetic flux density, magnetization, eddy current, losses, force and torque.

Today's challenges in the EM FEA are material modeling and high speed calculation for large scale models. Since material characteristics are basically given parameters for the equation[14)], the accuracy of the characteristics will directly affect the accuracy of the solution. On the other hand, behavior of material is so complex[15)] that it is difficult to have a material model which reproduces the behavior with reasonable costs. Although it is, of course, possible to use

the micro magnetic simulation techniques such as the material model, there are two significant problems which are enormous calculation cost and the fact that it is difficult to obtain parameters for the model by usual material measurements. Eventually, relatively simple material models, which is costless and can be constructed with measurable parameters, are employed in today's practical situations accepting certain inaccuracy. In this context, several new material models have been proposed and being examined.
The high speed calculation is natural sequence of pursuing highly accurate solution which is required for today's sophisticated detail design in advanced applications such as EV/HV. The main stream of speeding up is utilizing multi-/many cores equipped in the latest computing systems, that is parallel computing. However, the calculation scheme of EM FEM is not easily parallelized by its nature and many new ideas are required.
The EM FEA is actively used for wide range of applications and is still attracting users because of its powerful and flexible functionality. The technical challenges are going on to enhance the functionality and it is still evolving.

References

1) Takashi Yamada, Development of electromagnetic simulation software in rotating electric machine design, JRI Solutions Limited, The Papers of Technical Meeting on Rotating Machinery, IEE Japan, Vol. RM-07-142, October 2007
2) M. V. K. Chari, Finite Element Analysis of Electrical Machinery and Devices, General Electric Company, IEEE Transactions on Magnetics, Vol. Mag-16, No 5, September 1980
3) M. Watanabe, S. Shirai and M. Fukushima, Computation of Deflection Defocusing in CRT Electron Beams with Three-dimentional Nonlinear Analysis of Magnetic Fields, Hitachi Ltd., 1998 International Display Research Conference
4) J. Nakata, M. Nakajima, T. Hosokawa, T. Kitayama, Three-dimensional magnetic field analysis of superconducting 180° bending magnets, NTT Corp., IEEE Transactions on Magnetics, Vol. 26, No 2, March 1990, pp 913-916
5) Hideyuki Watanabe, Promotion to Spread JMAG to Actuator Development and Applications, Keihin Corporation, JMAG Users Conference Proceedings 2005
6) Yasushi Kanai, Niigata Institute of Technology, Numerical Simulation Analysis of Magnetic Recording, JMAG Users Conference Proceedings 1998
7) Miyoko Okutani, Optimization Method for Inner Magnetic Shield in CRT, Matsushita Electric Industrial Co., Ltd., JMAG Users Conference Proceedings 2002
8) Takashi Horino, Computer Analysis of Dual Frequency Induction Heating using JMAG-Studio, NETUREN CO.,LTD., JMAG Users Conference Proceedings 2007
9) M.Sato, A.Kameari, K.Koganezawa, N.Setsuo, Analysis of Eddy Current Testing (ECT) by FEM using edge elements, The Papers of Joint Technical Meeting on SA and RM, IEE JAPAN, Vol. SA-95-12, RM-95-74, August 1995
10) Akio Yamagiwa, Analysis of a Permanent Magnet Motor, DAIKIN INDUSTRIES, Ltd., JMAG Users Conference Proceedings 1997
11) Takeshi Ikemi, Development of High power & High efficiency Motor for EV using magnetic field analysis, Nissan Motor Co.,LTD, JMAG Users Conference Proceedings 2013
12) Ryoji Mizutani, The Motor Control Technologies for New-Generation Prius, TOYOTA MOTOR CORPORATION, JMAG Users Conference Proceedings 2004
13) Masaaki Kaizuka, Development of 2005 Model Year ACCORD Hybrid, Honda R&D Co.,Ltd., JMAG Users Conference Proceedings 2005
14) Koji Fujiwara, Key Points of Numerical Analysis -Present Challenges Related to Material Properties-, Okayama University, JMAG Users Conference Proceedings 1998
15) Chikara Kaido, Handling Cores and Core Materials in Numerical Analyses for Motor Design and Analysis, Kitakyushu National College of Technology, JMAG Users Conference Proceedings 2013